

Communication

Spherical Activated Carbons with High Mechanical Strength Directly Prepared from Selected Spherical Seeds

Ana Amorós-Pérez, Laura Cano-Casanova, Mohammed Ouzzine, Mónica Rufete-Beneite, Aroldo José Romero-Anaya , María Ángeles Lillo-Ródenas *  and Ángel Linares-Solano

MCMA Group, Department of Inorganic Chemistry and Materials Institute, University of Alicante, E-03080 Alicante, Spain; ana.amoros@ua.es (A.A.-P.); laura.cano@ua.es (L.C.-C.); ouzzine_mohamed@yahoo.fr (M.O.); monica.rufete@ua.es (M.R.-B.); ajromero@ua.es (A.J.R.-A.); linares@ua.es (A.L.-S.)

* Correspondence: mlillo@ua.es; Tel.: +34-965-90-35-45; Fax: +34-965-90-34-54

Received: 21 March 2018; Accepted: 4 May 2018; Published: 10 May 2018



Abstract: In the present manuscript, the preparation of spherical activated carbons (SACs) with suitable adsorption properties and high mechanical strength is reported, taking advantage of the retention of the spherical shape by the raw precursors. An easy procedure (carbonization followed by CO₂ activation) has been applied over a selection of three natural seeds, with a well-defined spherical shape and thermal stability: *Rhamnus alaternus* (RA), *Osyris lanceolate* (OL), and *Canna indica* (CI). After the carbonization-activation procedures, RA and CI, maintained their original spherical shapes and integrity, although a reduction in diameter around 48% and 25%, respectively, was observed. The porosity of the resulting SACs could be tuned as function of the activation temperature and time, leading to a spherical activated carbon with surface area up to 1600 m²/g and mechanical strength similar to those of commercial activated carbons.

Keywords: spherical seeds; spherical activated carbons; activation; microporosity; mechanical properties

1. Introduction

Spherical activated carbons (SACs) are very interesting materials, which are attracting great attention because of their outstanding physical properties, such as wear resistance, mechanical strength, good adsorption performance, purity, low ash content, smooth surface, good fluidity, good packaging, low pressure drop, high bulk density, high micropore volume and tunable pore size distribution [1–5]. All these features make SACs suitable for various applications like blood purification, catalysts support, chemical protective clothing [2,6,7], in adsorption processes; both in gas phase (e.g., toluene, CO₂, CH₄ and H₂) [5,8–10] and solution (e.g., phenol) [11], as supercapacitors [12,13], in medicine for poison adsorption in living organisms [14], as catalyst supports for hydrogenation reactions [15,16], etc.

SACs can be prepared using several methods: by polymerization reactions [17], by agglomeration from mixtures of resin and activated carbon [18] or by hydrothermal synthesis [19–23]. All these methods imply the use of expensive or synthetic precursors (such as aerogels [17], divinylbenzene-derived polymers [24] and urea/formaldehyde resin [25]). However, nowadays it is common to look for cheaper precursors, such as coals [4], lignocellulosic materials [19–21] and carbohydrates [22,26–29].

Herein we present the preparation of SACs with high mechanical strength and tunable porosity from spherical seeds using an easy, cheap and a well-known method. This simple route allows the valorization of inexpensive and available biomass precursors, such as not edible seeds, to convert them in potentially useful and valuable materials like SACs. In particular, we focused our interest

on the selected seeds that combine simultaneous spherical shape and thermal stability, and cover a wide range of diameters (from 1 to 7 mm). It should be highlighted that the size of the final materials would depend on the size of the used precursor. Among the tested spherical seeds, which accomplish these requirements (Table 1), the study was focused on three of them: *Rhamnus alaternus* (RA), *Osyris lanceolate* (OL), and *Canna indica* (CI) (Figure 1).

Table 1. Common and scientific names of the selected spherical seeds and their diameters.

Common Name	Scientific Name	Mean Diameter (mm)
Poppy	<i>Papaver rhoeas</i>	1
Amaranth	<i>Amaranthus hypochondriacus</i>	1
Millet	<i>Panicum miliaceum</i>	2
Mustard	<i>Sinapis alba</i>	3
Black pepper	<i>Piper nigrum</i>	4
False pepper	<i>Schinus molle</i>	4
Palm	<i>Phoenix dactylifera</i>	5
Indian shot	<i>Canna indica</i>	5
African sandalwood	<i>Osyris lanceolate</i>	5
Phoenician juniper	<i>Juniperus phoenicea</i>	6
Mediterranean buckthorn	<i>Rhamnus alaternus</i>	7
Prickly juniper	<i>Juniperus oxycedrus</i>	7

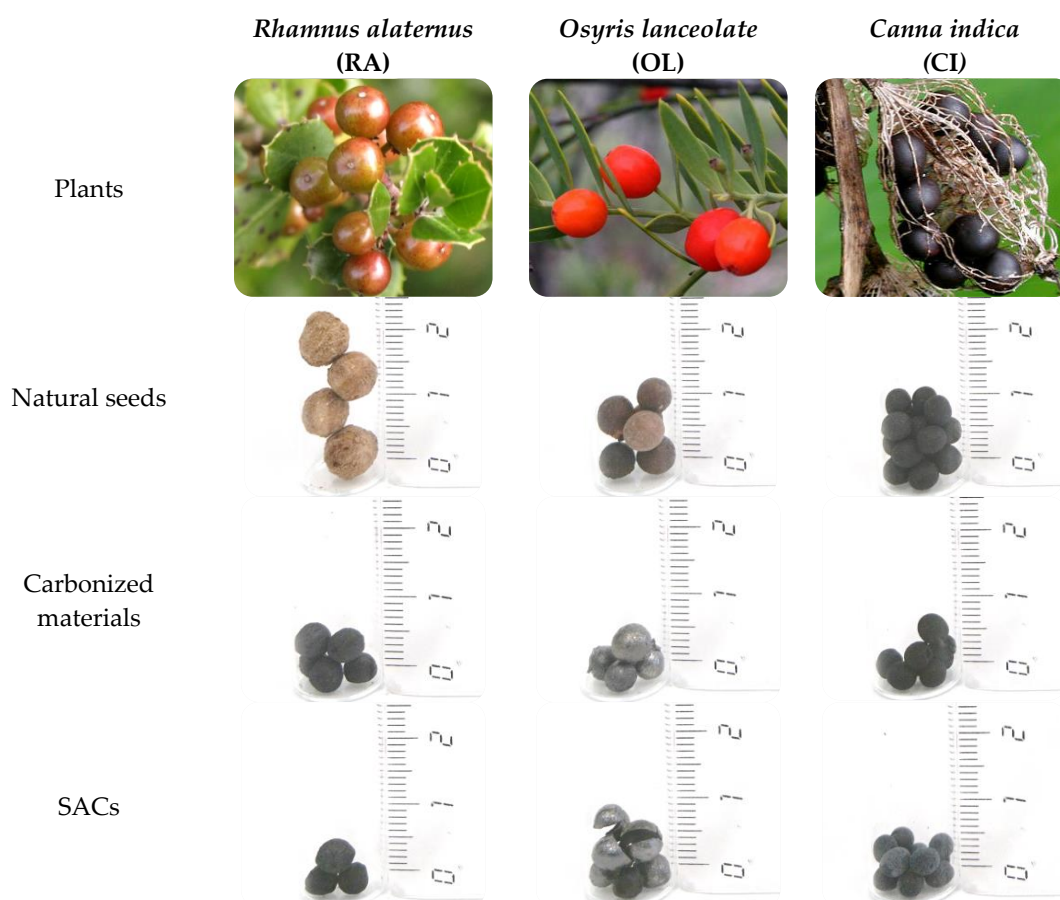


Figure 1. Natural seeds used as precursors for SACs preparation, together with the carbonized and activated spherical materials prepared from them.

2. Materials and Methods

2.1. Methodology

2.1.1. Carbonization Process

All the seeds were initially dried in an oven at 110 °C for 3 h. For the carbonization process, 2 g of such dried seeds were heated up to 850 °C, held for 2 h, in a horizontal furnace with N₂ flow of 300 mL/min, and a heating rate of 5 °C/min. The corresponding carbonization yields are summarized in Table 2.

Table 2. Mechanical strength (expressed as the percentage of the remaining mass after sieving, SRM%, see Section 2.2.3.) of the natural seeds and carbonization yields, textural properties and mechanical strength (SRM%) of the materials after carbonization.

Precursor	SRM ^a (%)	Yield ^b (%)	V _{DR} (N ₂) ^c (cm ³ /g)	V _{DR} (CO ₂) ^d (cm ³ /g)	SRM ^e (%)
RA	99.1	30	0.01	0.18	98.8
OL	99.9	21	0.01	0.19	99.4
CI	99.0	22	0.02	0.20	98.7

^a SRM, remaining mass after sieving the natural spherical seeds, as percentage. ^b Yield, yield of carbonization process, as percentage. ^c V_{DR} (N₂), total micropore volume, obtained applying the Dubinin-Raduskevich method to data of N₂ adsorption isotherm at −196 °C. ^d V_{DR} (CO₂), narrow micropore volume, obtained applying the Dubinin-Raduskevich method to data of CO₂ adsorption isotherm at 0 °C. ^e SRM, remaining mass after sieving the carbonized materials, as percentage.

2.1.2. Activation Process

Carbonized seeds were activated using CO₂ in order to develop their porosity, using a CO₂ flow of 80 mL/min. To study the effect of temperature and time on the activation process, the samples were heated at 5 °C/min up to different temperatures: 800, 850, or 880 °C, and such temperatures were maintained for various fixed times, as described in Table 3.

Table 3. Activation conditions, activation percentages, SRM values and textural properties of some activated samples.

Precursor	T (°C)	t (h)	Burn-off (%)	S _{BET} ^a (m ² /g)	V _{DR} (N ₂) ^b (cm ³ /g)	V _{DR} (CO ₂) ^c (cm ³ /g)	V _{meso} ^d (cm ³ /g)	SRM ^e (%)	V _{N₂} −V _{CO₂} ^g (cm ³ /g)
RA	800	10	6	492	0.20	0.25	0.03	NM ^f	< 0
	800	30	26	812	0.28	0.36	0.02	97.8	< 0
	800	40	33	889	0.40	0.33	0.03	NM ^f	0.07
	850	10	33	874	0.39	0.37	0.02	NM ^f	0.02
CI	800	5	33	856	0.39	0.35	0.05	94.9	0.04
	880	3	89	1616	0.64	0.37	0.19	85.3	0.27

^a S_{BET}, BET surface area, obtained applying the BET method to data of N₂ adsorption isotherm at −196 °C. ^b V_{DR} (N₂), total micropore volume, obtained applying the Dubinin–Raduskevich method to data of N₂ adsorption isotherm at −196 °C. ^c V_{DR} (CO₂), narrow micropore volume, obtained applying the Dubinin–Raduskevich method to data of CO₂ adsorption isotherm at 0 °C. ^d V_{meso}, mesopore volume, obtained from N₂ adsorbed as liquid at P/P₀ = 0.9 minus the adsorbed volume at P/P₀ = 0.2 [30]. ^e SRM, remaining mass after sieving the activated materials, as percentage. ^f NM: not measured. ^g V_{N₂}−V_{CO₂}, difference between V_{DR} (N₂) and V_{DR} (CO₂).

2.2. Characterization

2.2.1. Morphology

Morphology of the original, carbonized and activated samples was characterized by Scanning Electron Microscopy (SEM) in a JSM-840 microscope (JEOL, Tokyo, Japan) with a scintillator–photomultiplier type secondary electron detector.

2.2.2. Surface Area and Pore Volumes

Textural characterization of precursors, carbonized and activated materials was performed using N_2 adsorption at $-196\text{ }^\circ\text{C}$ [31] and CO_2 at $0\text{ }^\circ\text{C}$ [32] in a volumetric Autosorb-6B apparatus from Quantachrome. Before analysis, the samples were degassed at $250\text{ }^\circ\text{C}$ for 4 h. The BET equation was applied to the nitrogen adsorption isotherm in the low-pressure region (relative pressure between 0.05–0.25) to get the apparent BET surface area, S_{BET} [30]. The Dubinin–Radushkevich equation was applied to the nitrogen adsorption isotherm to determine the total micropore volume ($V_{DR}(N_2)$ corresponding to micropores of size below 2 nm) and to the carbon dioxide adsorption isotherms to determine narrow micropore volume ($V_{DR}(CO_2)$, corresponding to micropores of size below 0.7 nm) [33]. Mesopore volume, V_{meso} , corresponding to pores between 2 and 20 nm, was estimated from N_2 adsorbed as liquid at $P/P_0 = 0.9$ minus the volume adsorbed at $P/P_0 = 0.2$ [30]. The difference between $V_{DR}(N_2)$ and $V_{DR}(CO_2)$ was calculated as an estimation of the micropore size distribution [30,31].

2.2.3. Mechanical Properties

The mechanical strength, defined as SRM%, was estimated by a method developed in our laboratory that consists of the evaluation of the sample mass remaining in a sieve after vigorous shaking (Figure 2). Thus, for each test, a known quantity of material was put in a cylindrical vial together with 15 stainless steel balls (Figure 2a). These vials were placed horizontally in a polymer mold used as immobilizing support (Figure 2b), which was placed in an electromagnetic sieve shaker CIPSA RP08 Ø200/203 for 20 min at power number 8 (equivalent to the shaking speed of 1.8 mm of vibration amplitude per second) (Figure 2c). Then, the samples were sieved using a sieve (300 μm) and the resulting residue (the sample not converted to dust in the sieving step) was weighed (Figure 2d). The mechanical strength was expressed as the percentage of the remaining mass after sieving (SRM%). The validation of this method was performed by analyzing the mechanical properties of several commercial activated carbons (Table 4), and such values were used as reference to confirm that the mechanical properties of our SACs are similar to those of their commercial counterparts. Note that the SRM values for the selected commercial ACs are in the range between 72% and 97%. The analysis of the mechanical properties was performed for the precursors, carbonized materials (Table 2) and for the activated ones (Table 3).



Figure 2. Depiction of materials and procedure for the mechanical strength evaluation of the samples: (a) a weighted sample was sieved using in 300 μm sieve and put in a vial; (b) 15 steel balls were also incorporated in the vial, which was then placed in a polymer mold; (c) the molds were placed in the sieve shaker during 20 min; (d) the sample was sieved again in a 300 μm sieve and the residue (the sample not converted to dust in the sieving step) was collected and weighed to calculate the sample remaining mass percentage (SRM%).

Table 4. Textural properties and SRM values of some commercial activated carbons.

Name	Commercial Name	Morphology and Size	S _{BET} ^a (m ² /g)	V _{DR} (N ₂) ^b (cm ³ /g)	V _{DR} (CO ₂) ^c (cm ³ /g)	V _{meso} ^d (cm ³ /g)	SRM (%)
CW	Mead Westvaco, WVA1100	Granular (10 × 25 mesh)	1796	0.72	0.34	0.42	72
CK	Kureha Corporation carbon from petroleum pith	Spherical (0.75 μm)	1185	0.57	0.42	0.02	97
ROX	NORIT® ROX	Pellets (0.8 mm)	1354	0.60	0.40	0.07	92

^a S_{BET}, BET surface area, obtained applying the BET method to data of N₂ adsorption isotherm at −196 °C. ^b V_{DR} (N₂), total micropore volume, obtained applying the Dubinin-Raduskevich method to data of N₂ adsorption isotherm at −196 °C. ^c V_{DR} (CO₂), narrow micropore volume, obtained applying the Dubinin-Raduskevich method to data of CO₂ adsorption isotherm at 0 °C. ^d V_{meso}, mesopore volume, obtained from N₂ adsorbed as liquid at P/P₀ = 0.9 minus the adsorbed volume at P/P₀ = 0.2 [30].

3. Results

Figure 3 shows that the retention of the desired original spherical shape during the carbonization process was achieved for these three seeds, though this step generally led to a decrease in the diameter of the materials. Such variation depends on the type of seed: for RA the size was significantly reduced (around 3 mm, which represents 40% reduction), while CI and OL were only slightly shortened (in both cases about 1 mm, around 20%). This could be related with the intrinsic natural differences in the composition of the seeds.

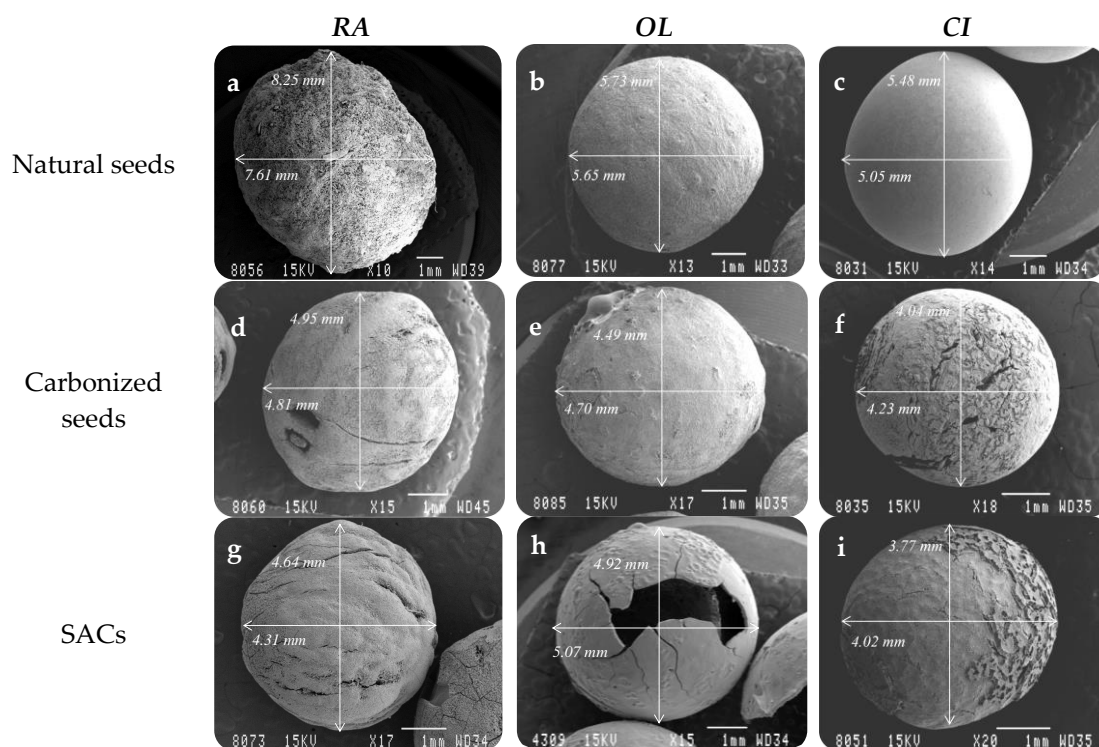


Figure 3. SEM images of precursors, carbonized materials and final SACs. Experimental preparation conditions of the materials: (a–c) dried at 110 °C for 3 h; (d–f) carbonized at 850 °C for 2 h in 300 mL/min N₂ flow; (g) activated at 800 °C for 30 h using 80 mL/min CO₂ flow; (h) activated at 800 °C for 2 h in 80 mL/min CO₂ flow; (i) activated at 800 °C for 5 h in 80 mL/min CO₂ flow.

Table 2 reports carbonization yields and values of mechanical properties (SRM%) for CI, RA, and OL carbonized seeds, together with SRM values for the precursors, as reference. It shows that: (i) the carbonization yields ranged from 21 to 30%, which is in the range of typical values expected for lignocellulosic materials [34]; (ii) micropore volumes determined by CO₂ adsorption were larger

than those measured by N_2 , indicating that the mean micropore sizes were below 0.7 nm [31], and (iii) SRM values were higher than 98.7%, indicating that the samples possess high mechanical resistance. Such porous texture, together with the mechanical properties, made these carbonized materials potentially useful as spherical carbon molecular sieves.

The conditions of the activation process were also optimized in order to obtain similar burn-off percentage (around 30%) and maintain the spherical morphology. Figure 3 shows that RA and CI seeds retained their original shape after activation, and their sizes were minimally affected (around 0.5 mm (8% reduction with respect to the size) before the activation, and 0.2 mm (5%), respectively). Only OL seeds were broken after activation, and this occurred for all the explored activation conditions. Hence, from OL only spherical carbonized materials could be prepared. It is important to mention that the carbonized and activated materials from both RA and CI remained physically intact (without cracks) and the same occurred for carbonized OL, whereas only the material obtained from OL, after the activation process showed cracks, that can be visually distinguished.

With respect to the activation yields (Table 3), CI was the more reactive candidate, since a shorter activation time was required to get 33% burn-off. For the RA precursor, as expected, the burn-off percentage at constant temperature increases proportionally with the reaction time. Interestingly, the desired activation percentage (33%) could also be achieved for RA using higher temperatures (850 °C instead of 800 °C) and shorter times (10 h instead of 40 h).

Regarding the textural properties, Table 3 shows that, for RA seeds, although there exists a linear relationship between the activation time and the burn-off percentage, no direct correlation was found when analyzing the effect of the activation time on the porosity development. For this precursor, the same burn-off percentage, 33%, and similar surface area values (about 880 m^2/g) have been obtained using different combinations of activation temperature and time. Low activation times (10 and 30 h) led to materials with the mean micropore sizes below 0.7 nm, whereas the micropore size was around that value for larger activation time and temperature.

Similar experimental conditions screening for CI precursor highlighted that higher adsorption capacities can be developed from it, which reached 1616 m^2/g when treating up to 880 °C for 3 h. For the CI activated material with surface area above 1600 m^2/g , the fact that total micropore volume determined by N_2 adsorption is much larger than that measured by CO_2 , is indicative of the average pore size above 0.7–1 nm [30].

By comparing SRM values for natural and carbonized materials in Table 2, it can be observed that natural precursors show slightly higher mechanical strength than the corresponding carbonized spheres. Table 3 contains the SRM values for SACs, indicating that their mechanical properties are only slightly reduced after the activation process. This is probably due to the high number of heteroatoms linked to the carbon material, and eliminated during the activation [35]. However, SRM values are in the range of 95% for samples with areas around 800 m^2/g , and about 85% when the BET surface area surpasses 1600 m^2/g , which indicated that the samples generally display significant mechanical properties that lie in the range of the selected common commercial references (CW, CK and ROX) (Table 4 and Figure 4).

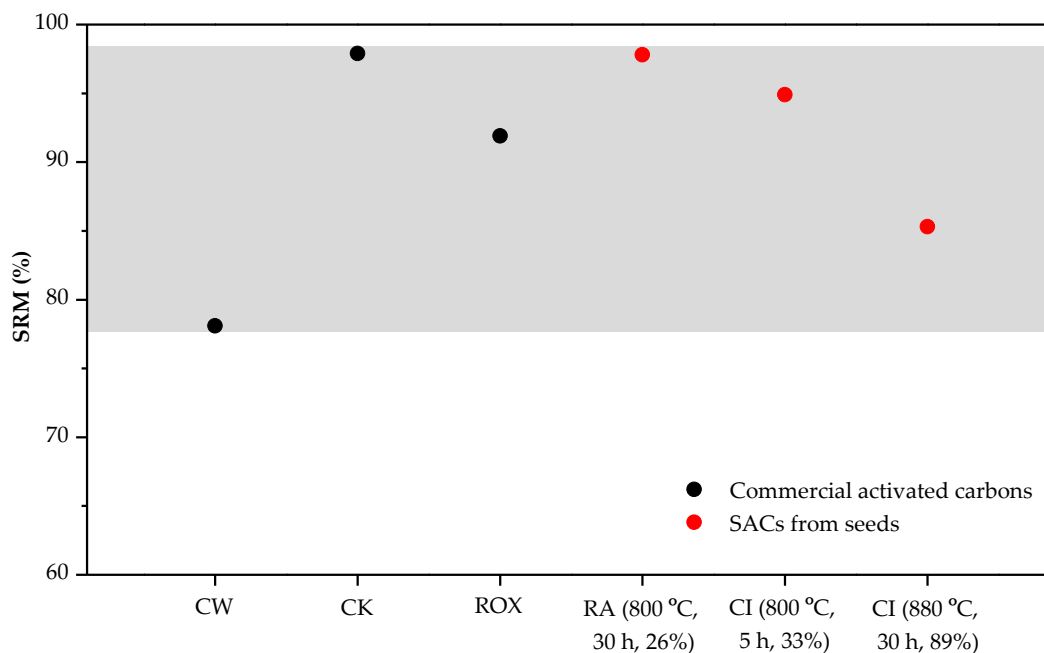


Figure 4. SRM values for commercial activated carbons (black color) and for some activated seeds prepared in this work (orange color).

4. Conclusions

In this work spherical activated carbons with high mechanical strength and well-developed porosity were prepared while maintaining the spherical shape of the natural seeds, selected as carbon precursors. The three reported candidates: RA, OL and CI, could be successfully converted into spherical activated carbon materials using a well-known, simple and cheap method and, additionally, CI and RA maintained their original spherical shapes and integrity all along the activation process, avoiding breakage. Their diameter sizes were notably reduced after the carbonization step and only slightly affected by the activation process. The mechanical properties for all the activated materials were found to be similar to those of common commercial activated carbons with different morphologies (granular, spherical and pellets). Interestingly, depending on the precursor and/or on the activation conditions, significant differences in porosity development and micropore size distributions were obtained, reaching specific surface areas up to 1600 m²/g. The interesting properties of the prepared materials, together with their spherical morphology, make them interesting candidates for many applications.

Author Contributions: Á.L.-S. conceived and designed the experiments; A.A.-P., L.C.-C., M.O., M.R.-B. and A.J.R.-A. performed the experiments; A.A.-P., L.C.-C., M.O., M.A.L.-R. and Á.L.-S. analyzed the data; A.A.-P., M.O., A.J.R.-A., M.A.L.-R. and Á.L.-S. contributed reagents/materials/analysis tools; A.A.-P., A.J.R.-A., M.A.L.-R. and Á.L.-S. wrote the paper.

Funding: This research received no external funding.

Acknowledgments: The authors thank the Spanish Ministry of Economy and Competitiveness (MINECO) and FEDER, project of reference CTQ2015-66080-R, GV/FEDER (PROMETEOII/2014/010) and University of Alicante (VIGROB-136) for financial support. Pilar Garcia Cardona, from Universidad Nacional de Colombia-Medellin is acknowledged for providing some of the spherical materials.

Conflicts of Interest: The authors declare no conflict of interest.

References

1. Liu, J.; Wickramaratne, N.P.; Qiao, S.Z.; Jaroniec, M. Molecular-based design and emerging applications of nanoporous carbon spheres. *Nat. Mater.* **2015**, *14*, 763–774. [[CrossRef](#)] [[PubMed](#)]
2. Liu, Z.; Ling, L.; Qiao, W.; Liu, L. Effect of hydrogen on the mesopore development of pitch-based spherical activated carbon containing iron during activation by steam. *Carbon* **1999**, *37*, 2063–2066. [[CrossRef](#)]
3. Liang, X.; Zhang, R.; Liu, C.; Liu, X.; Qiao, W.; Zhan, L.; Ling, L. Preparation of polystyrene-based activated carbon spheres and their adsorption of dibenzothiophene. *New Carbon Mater.* **2009**, *9*, 8–13. [[CrossRef](#)]
4. Gryglewicz, G.; Grabas, K.; Lorenc-Grabowska, E. Preparation and characterization of spherical activated carbons from oil agglomerated bituminous coals for removing organic impurities from water. *Carbon* **2002**, *40*, 2403–2411. [[CrossRef](#)]
5. Romero-Anaya, A.J.; Lillo-Ródenas, M.A.; Linares-Solano, A. Spherical activated carbons for low concentration toluene adsorption. *Carbon* **2010**, *48*, 2625–2633. [[CrossRef](#)]
6. Yenisoy-Karakaş, S.; Aygün, A.; Güneş, M.; Tahtasakal, E. Physical and chemical characteristics of polymer-based spherical activated carbon and its ability to adsorb organics. *Carbon* **2004**, *42*, 477–484. [[CrossRef](#)]
7. Lee, C.; Hsu, S. Preparation of spherical encapsulation of activated carbons and their adsorption capacity of typical uremic toxins. *J. Biomed. Mater. Res.* **1990**, *24*, 243–258. [[CrossRef](#)] [[PubMed](#)]
8. Wickramaratne, N.P.; Jaroniec, M. Activated carbon spheres for CO₂ adsorption. *Appl. Mater. Interfaces* **2013**, *5*, 1849–1855. [[CrossRef](#)] [[PubMed](#)]
9. Romero-Anaya, A.J.; Lillo-Ródenas, M.A.; Linares-Solano, A. Activation of a spherical carbon for toluene adsorption at low concentration. *Carbon* **2014**, *77*, 616–626. [[CrossRef](#)]
10. Li, Y.; Li, D.; Rao, Y.; Zhao, X.; Wu, M. Superior CO₂, CH₄, and H₂ uptakes over ultrahigh-surface-area carbon spheres prepared from sustainable biomass-derived char by CO₂ activation. *Carbon* **2016**, *105*, 454–462. [[CrossRef](#)]
11. Liu, C.; Liang, X.; Liu, X.; Wang, Q.; Teng, N.; Zhan, L.; Zhang, R.; Qiao, W.; Ling, L. Wettability modification of pitch-based spherical activated carbon by air oxidation and its effects on phenol adsorption. *Appl. Surf. Sci.* **2008**, *254*, 2659–2665. [[CrossRef](#)]
12. Xuan, H.; Wang, Y.; Lin, G.; Wang, F.; Zhou, L.; Dong, X.; Chen, Z. Air-assisted activation strategy for porous carbon spheres to give enhanced electrochemical performance. *RSC Adv.* **2016**, *6*, 15313–15319. [[CrossRef](#)]
13. Sevilla, M.; Fuertes, A.B. A green approach to high-performance supercapacitor electrodes: The chemical activation of hydrochar with potassium bicarbonate. *ChemSusChem* **2016**, 1880–1888. [[CrossRef](#)] [[PubMed](#)]
14. Tsivadze, A.Y.; Gur'yanov, V.V.; Petukhova, G.A. Preparation of spherical activated carbon from furfural, its properties and prospective applications in medicine and the national economy. *Prot. Met. Phys. Chem. Surf.* **2011**, *47*, 612–620. [[CrossRef](#)]
15. Bo, B.; Wasserscheid, P.; Etzold, B.J. Polymer-based spherical activated carbon as easy-to-handle catalyst support for hydrogenation reactions. *Chem. Eng. Technol.* **2016**, *39*, 276–284. [[CrossRef](#)]
16. Rufete-Beneite, M.; Román-Martínez, M.C.; Linares-Solano, A. Insight into the immobilization of ionic liquids on porous carbons. *Carbon* **2014**, *77*, 947–957. [[CrossRef](#)]
17. Long, D.; Zhang, R.; Qiao, W.; Zhang, L.; Liang, X.; Ling, L. Biomolecular adsorption behavior on spherical carbon aerogels with various mesopore sizes. *J. Colloid Interface Sci.* **2009**, *331*, 40–46. [[CrossRef](#)] [[PubMed](#)]
18. Oh, W.C.; Kim, J.G.; Kim, H.; Chen, M.L.; Zhang, F.J.; Zhang, K.; Meng, Z. Preparation of spherical activated carbon and their physicochemical properties. *J. Korean Ceram. Soc.* **2009**, *46*, 568–573. [[CrossRef](#)]
19. Luo, G.; Shi, W.; Chen, X.; Ni, W.; Strong, P.J.; Jia, Y.; Wang, H. Hydrothermal conversion of water lettuce biomass at 473 or 523 K. *Biomass Bioenergy* **2011**, *35*, 4855–4861. [[CrossRef](#)]
20. Hoekman, S.K.; Broch, A.; Robbins, C. Hydrothermal Carbonization of Lignocellulosic Biomass. *Energy Fuels* **2014**, *25*, 1802–1810. [[CrossRef](#)]
21. Sevilla, M.; Maciá-Agulló, J.A.; Fuertes, A.B. Hydrothermal carbonization of biomass as a route for the sequestration of CO₂: Chemical and structural properties of the carbonized products. *Biomass Bioenergy* **2011**, *35*, 3152–3159. [[CrossRef](#)]
22. Sun, X.; Li, Y. Ga₂O₃ and GaN semiconductor hollow spheres. *Angew. Chem. Int. Ed.* **2004**, *43*, 3827–3831. [[CrossRef](#)] [[PubMed](#)]

23. Bedin, K.C.; Cazetta, A.L.; Souza, I.P.A.F.; Pezoti, O.; Souza, L.S.; Souza, P.S.C.; Yokoyama, J.T.C.; Almeida, V.C. Porosity enhancement of spherical activated carbon: Influence and optimization of hydrothermal synthesis conditions using response surface methodology. *J. Environ. Chem. Eng.* **2018**, *6*, 991–999. [[CrossRef](#)]
24. Zhu, Z.; Li, A.; Yan, L.; Liu, F.; Zhang, Q. Preparation and characterization of highly mesoporous spherical activated carbons from divinylbenzene-derived polymer by $ZnCl_2$ activation. *J. Colloid Interface Sci.* **2007**, *316*, 628–634. [[CrossRef](#)] [[PubMed](#)]
25. Wang, D.; Chen, M.; Wang, C.; Bai, J.; Zheng, J. Synthesis of carbon microspheres from urea formaldehyde resin. *Mater. Lett.* **2011**, *65*, 1069–1072. [[CrossRef](#)]
26. Yao, C.; Shin, Y.; Wang, L.Q.; Windisch, C.F.; Samuels, W.D.; Arey, B.W.; Wang, C.; Risen, W.M.; Exarhos, G.J. Hydrothermal dehydration of aqueous fructose solutions in a closed system. *J. Phys. Chem. C* **2007**, *111*, 15141–15145. [[CrossRef](#)]
27. Sevilla, M.; Fuertes, A.B. The production of carbon materials by hydrothermal carbonization of cellulose. *Carbon* **2009**, *47*, 2281–2289. [[CrossRef](#)]
28. Wang, F.L.; Pang, L.L.; Jiang, Y.Y.; Chen, B.; Lin, D.; Lun, N.; Zhu, H.-L.; Liu, R.; Meng, X.L.; Wang, Y.; et al. Simple synthesis of hollow carbon spheres from glucose. *Mater. Lett.* **2009**, *63*, 2564–2566. [[CrossRef](#)]
29. Romero-Anaya, A.J.; Ouzzine, M.; Lillo-Ródenas, M.A.; Linares-Solano, A. Spherical carbons: Synthesis, characterization and activation processes. *Carbon* **2014**, *68*, 296–307. [[CrossRef](#)]
30. Rodríguez-Reinoso, F.; Linares-Solano, A. *Microporous Structure of Activated Carbons as Revealed by Adsorption Methods*; Thrower, P.A., Ed.; Marcel Dekker Inc.: New York, NY, USA, 1989; Volume 21, ISBN 0-8247-7939-8.
31. Linares-Solano, Á.; Salinas-Martínez de Lecea, C.; Alcañiz-Monge, J.; Cazorla-Amorós, D. Further advances in the characterization of microporous carbons by physical adsorption of gases. *Tanso* **1998**, *185*, 316–325. [[CrossRef](#)]
32. Cazorla-Amorós, D.; Alcañiz-Monge, J.; Linares-Solano, A. Characterization of activated carbon fibers by CO_2 adsorption. *Langmuir* **1996**, *12*, 2820–2824. [[CrossRef](#)]
33. Lillo-Ródenas, M.A.; Marco-Lozar, J.P.; Cazorla-Amorós, D.; Linares-Solano, A. Activated carbons prepared by pyrolysis of mixtures of carbon precursor/alkaline hydroxide. *J. Anal. Appl. Pyrolysis* **2007**, *80*, 166–174. [[CrossRef](#)]
34. Rodríguez-Reinoso, F.; Molina-Sabio, M. Activated carbons from lignocellulosic materials by chemical and/or physical activation: An overview. *Carbon* **1992**, *30*, 1111–1118. [[CrossRef](#)]
35. Contreras, M.S.; Páez, C.A.; Zubizarreta, L.; Léonard, A.; Blacher, S.; Olivera-Fuentes, C.G.; Arenillas, A.; Pirard, J.P.; Job, N. A comparison of physical activation of carbon xerogels with carbon dioxide with chemical activation using hydroxides. *Carbon* **2010**, *48*, 3157–3168. [[CrossRef](#)]

